AIAA 2002-0773

THE STRUCTURE OF THE DETONATION FRONT IN GASES

J.E. Shepherd, F. Pintgen, J.M. Austin, C.A. Eckett
Graduate Aeronautical Laboratories, California Institute of Technology, Pasadena, CA 91125

40th AIAA
Aerospace Sciences Meeting and Exhibit
14-17 January 2002/Reno, NV

THE STRUCTURE OF THE DETONATION FRONT IN GASES

J.E. Shepherd, F. Pintgen, J.M. Austin, C.A. Eckett
Graduate Aeronautical Laboratories, California Institute of Technology, Pasadena, CA 91125

We have carried out simultaneous visualizations of a chemical species (OH) and density gradients in the reaction zones of propagating detonations. We have directly imaged the characteristic shape of the chemical reaction zone and correlated this with the instability of the front. The observations have sufficient resolution to clearly see the variation in the reaction zone structure associated with leading shock velocity oscillations and complex flow behind the triple points associated with the intersection of transverse waves with the main front. Characteristic keystone-shaped regions of low reactivity are observed as predicted by previous analytical speculations. Observations on several types of mixtures are used to examine the issues of cellular regularity and the potential role of turbulence in the reaction process.

Nomenclature

$C_{p_{vN}}$	frozen post-shock heat capacity
E_a/RT_{vN}	nondimensional activation energy
L	cell length
M_{In}	normal Mach number, incident wave
M_{Mn}	normal Mach number, Mach stem
M_T	Mach number, transverse wave
M_{Tn}	normal Mach number, transverse wave
T_{vN}	frozen post-shock temperature
U_{CJ}	Chapman-Jouguet velocity
c_1	sound speed of reactants
p_1	initial pressure of reactants
$(x - x_o)$	axial distance through the cell from apex
Δ_{ZND}	induction zone length
β	shock angle
λ	cell width
θ	flow deflection angle
ρ_{vN}	frozen post-shock density
τ_T	induction time behind the transverse wave
τ_I	induction time behind the incident wave
ϕ	cell track angle
χ_{OH}	OH mole fraction

Introduction

ALL gaseous detonation waves propagating near the Chapman-Jouguet velocity are intrinsically unstable. The instability results in a quasi-periodic oscillation in the strength of the leading shock wave that is associated with a set of weak shock waves propagating transversely to the main front. As a consequence, the reaction zone region is spatially nonuniform and unsteady. Previous experimental studies of detonation waves have been primarily limited to point measurements of pressure, visualizations of the density field using schlieren or shadowgraph methods which integrate through the flowfield, or soot foil records of what are assumed to be triple point trajectories. These techniques are poorly suited to revealing the true structure of the detonation front. Further, the quantities of greatest interest, the concentrations of the chemical species, can at best be only indirectly inferred from such measurements.

Recognizing these limitations, Andresen et al.[1] applied the method of planar laser induced predissociated fluorescence (LIPF) in an effort to visualize a cross section of the OH concentration behind a detonation front in a hydrogen-oxygen-argon mixture. Although OH images were obtained, there was not sufficient spatial resolution to obtain any information other than the average spatial period of the oscillations in OH emission. One major difficulty that this study identified was the substantial amount of natural fluorescence that occurs in detonations and the importance of careful attention to reducing this in the final image in order to obtain high signal-to-noise ratios. Rayleigh scattering from a planar laser sheet was used by Anderson and Dabora[2] to image a cross section of the density field behind detonations propagating in hydrogen-oxygen-argon mixtures. Shock front shapes and quasi-periodic spatial fluctuations in density were observed that correlated with previous numerical and experimental studies. These results confirmed the density variations inferred from previous optical images and predicted by simulation. However, there was no insight provided into the chemical processes taking place in the reaction zone.

Recently, PLIF was applied with greater success to fast deflagrations and detonations in hydrogen-air mixtures by Eder.[3] Images of the chemical reaction front with sufficient spatial resolution and signal-to-noise ratio were achieved by using a tunable KrF laser with a pulse energy of 450 mJ exciting the OH-radical at a wavelength of 248 nm. A set of filters transmit the

---

fluorescence signal between a wavelength of 288 and 303 nm. In a round cross section facility of 66-mm diameter, Eder examined a variety of fast combustion processes in hydrogen-air mixtures with an equivalence ratio between 0.4 and 2.4 at atmospheric pressure. For marginal detonations with $\lambda/D \approx 1.6$, an irregular reaction front containing some unreacted regions was observed behind the leading shock wave. In detonations with $\lambda/D \leq 1$, the reaction front looked rather smooth and it was difficult to observe evidence of the cellular structure.

The experimental measurement of reaction structure in detonation waves remains an outstanding problem that we are actively investigating in our laboratory. Neither LIPF or Rayleigh scattering appeared to be promising given the relatively poor results in comparison to the success of LIF methods in elucidating the reaction zone structure of turbulent flames[4] and shock-induced combustion.[5–7] LIPF is a relatively low yield process and it was apparent that the signal-to-noise ratio was a significant issue with this technique. Rayleigh scattering is an extremely low yield method and also very difficult to use in most detonation tubes due to large numbers of particulates and soot buildup because of use with hydrocarbons or soot foil diagnostics. A much more promising technique is nonresonant LIF, pumping and detecting at different frequencies. By carefully choosing the parameters of the detonation and LIF system, we felt that it would be possible to overcome previous difficulties and image the details of the reaction zone structure.

Experimental Setup

The experiments were carried out using an 8-m long, 280-mm diameter detonation tube,[8] attached with a "cookie-cutter" to the 150-mm square test section described in Kaneshige.[9] Detonations are initiated with an exploding wire and a short section of acetylene-oxygen mixture injected immediately prior to the detonation event. Detonation pressure and velocity is monitored with a series of pressure transducers located along the length of the tube and in the test section. Stoichiometric mixtures of hydrogen and oxygen diluted with argon or nitrogen, initial pressure of 20 kPa, and nominal initial temperature of 25°C have been examined in the present study. The observation section is located approximately 7.5 m from the initiation point. The initiation system results in direct initiation with a highly repeatable function time and detonation velocities with 0.5% of the Chapman-Jouguet value. Schlieren images, pressure histories, and soot foil records indicate the detonations are fully-developed, self-sustaining waves within the test section.

The detonation reaction zone has been visualized by exciting OH fluorescence at about 284 nm with a planar light sheet and imaging the emitted light with an intensified charged-coupled device camera. Simultaneous observations with a laser shadowgraph have also been used in some tests.

The UV light for excitation of the OH molecules is produced by frequency doubling the output of an excimer-pumped dye laser. The excimer pump laser (XeCl Excimer, Lambda Physik Model 102) produces a 17 ns pulse of broadband light centered at 308 nm with a total energy of about 300 mJ. The dye laser (Scanmate 2E Lambda Physik) uses Coumarin 153 dye and a frequency doubler to obtain narrowband UV light with a total energy of about 6.5 mJ. The frequency of the dye laser was tuned to 284.008 nm, which is located half-way between two OH transitions: a) $A^2\Sigma^+$–$X^2\Pi_i(1,0)$ $Q_2(8)$ at 284.009 nm; b) $A^2\Sigma^+$–$X^2\Pi_i(1,0)$ $Q_1(9)$ at 284.007 nm. We chose these two transitions based on computations with the LIFBASE program[10] and repeated experimental trials. The offset of the dye laser frequency calibration was determined by scanning in frequency while measuring the fluorescence yield from a hydrogen diffusion flame in air, comparing the results to simulated scans with LIFBASE. The output of the frequency doubler was formed into a sheet by using a combination of cylindrical (focal length -25.4mm) and spherical lenses (focal length 1000 mm). The final usable height was about 80 mm and the thickness of about 0.3 mm was determined by burns on thermopaper. The light entered the test section through a slit and a quartz window in the end-wall of the test section.

The induced fluorescence emerged through a quartz window at 90 degrees to the sheet and was imaged on to a slow-scan 576×384 pixel CCD (Princeton Instruments ITE/ICCD-576) camera through a bandpass filter with a centerline of 313 nm and a 10 nm FWHM. The detected radiation is expected to be primarily due to (1,1) transitions[11] near 315 nm. Detection in this spectral region minimizes problems such as fluorescence trapping and ensures that the images will not be contaminated by Mie scattering or stray reflections from the test section of the incident light sheet. An image was formed by a 105-mm f/4.5 Nikkor UV-transmitting lens on to the microchannel plate, which was gated with a 100 ns pulse of 800 V. The gate signal to the camera was synchronized with the laser firing pulse, and the laser firing was coordinated with the detonation front location by using a programmable delay generator triggered from a pressure transducer located upstream of the visualization section. The signal from the pressure transducer is processed through a latching edge-detection trigger circuit to eliminate false triggers from the capacitor discharge system used to initiate the detonation.

Careful adjustment of the timing is essential to obtaining OH images since the excited state population quickly decays and the camera gate time must also be limited to maintain a high signal-to-noise ratio in the image. There are very high concentrations of OH behind a detonation front, and natural fluorescence is a significant source of noise. We found that the laser pulse must occur within the camera gate time in order to obtain an image of the laser induced fluorescence. In the present case, the operation of the pulse-forming circuit and thyratron switch in the excimer laser resulted in a delay of about 1200 ns between the trigger pulse and light output. A jitter of up to 200 ns can occur in the function of the thyratrons, requiring the timing to be tested and adjusted prior to each detonation experiment. The camera gate pulse was set to occur 50 ns prior to the nominal laser function time.

For simultaneous schlieren and PLIF images, the Q-switched, flash-lamp pumped ruby laser described by Akbar[8] was used to create a short (< 50 ns) light pulse at 693 nm. The light was formed into a collimated beam about 150 mm diameter, passed through the test section, and then imaged by a combination of mirrors and lenses on to high-speed instant (Polaroid 3000 ISO) film. The time between acquiring the schlieren and PLIF images is estimated to be less than 600 ns. The ICCD camera is placed just outside the optical path of the schlieren system and, therefore, views the laser sheet not normally but at a slight angle, causing the image to be slightly distorted. Images of a test pattern and postprocessing are used to correct this distortion and also align the two images.

Experimental Results

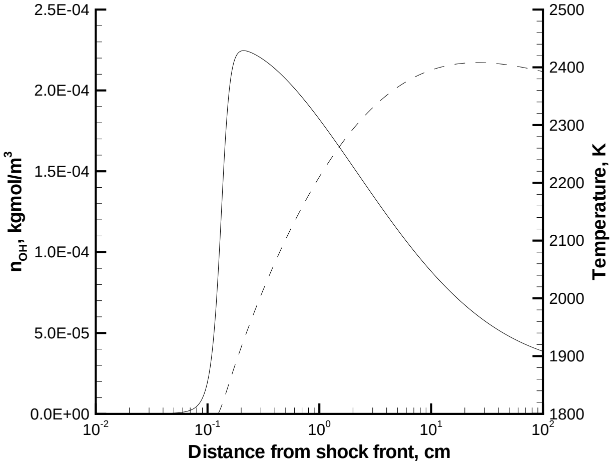

Fig. 1 OH number density and temperature ZND profiles for a CJ detonation in $2H_2$-O_2-17Ar at 20 kPa initial pressure. The solid line is OH number density, the dashed line corresponds to the temperature profile.

One OH image is obtained for each experiment. A selection of these images is shown in Figs. 3–5; the image is identified by the test number. The height of each image is approximately 80 mm and the detonation wave is traveling from left to right in all images. The detonation front instability exhibits seemingly random variations in the number of modes and the phasing of the transverse waves. For this reason, it is not possible to use repeated experiments to construct a coherent time sequence. It is also important to note that these images are qualitative rather than quantitative since we have not corrected for the effect of the laser beam nonuniformity or molecular effects such as quenching or time-dependence of the excited state population. The main value of the present results is in revealing the geometry of the OH fronts and enabling an interpretation in terms of gas dynamics and chemical reactions.

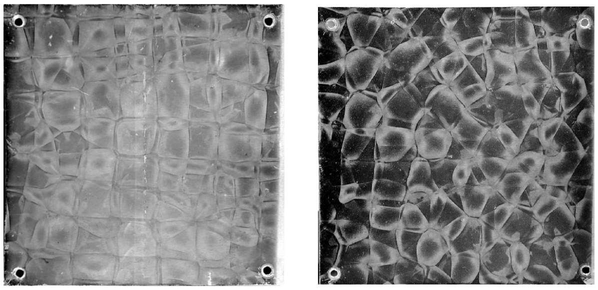

Fig. 2 Soot foils obtained from the end-wall of the test section, both are 2H2-O2-12Ar at 20 kPa. Note that the two planes of the detonation are not necessarily orthogonal to the text section walls, even for the same mixture.

A distinct OH concentration front is visible in all cases. Simulations of the reaction zone behind the shock front, discussed subsequently, indicate that the origin of the front is due to the sharp rise in the OH concentration at the end of the induction zone or region of radical chain reaction behind the main shock front. Note that even though OH is present in large concentrations at equilibrium, the fluorescence intensity decreases rapidly with increasing distance downstream (to the left in the images) from the front and there is significant radiation from only the first 20-30 mm behind the front. This can largely be explained by the fact that the PLIF signal is a function of the OH number density. Fig. 1 shows a ZND calculated OH number density profile through the reaction zone. A temperature profile is also shown. Other parameters influence the magnitude of the collected signal: the transition probability for absorption and spontaneous emission, the efficiency of the collection optics,[12] and the absorption of the light sheet energy by OH. Other potential influences include variations in the $X^2\Pi_i$ initial state population with thermodynamic state, and therefore with distance from the shock front and refraction of the incident light associated with the large refractive index variations near the absorption lines.

The geometry of the OH front is striking and some common features stand out. A single and particularly

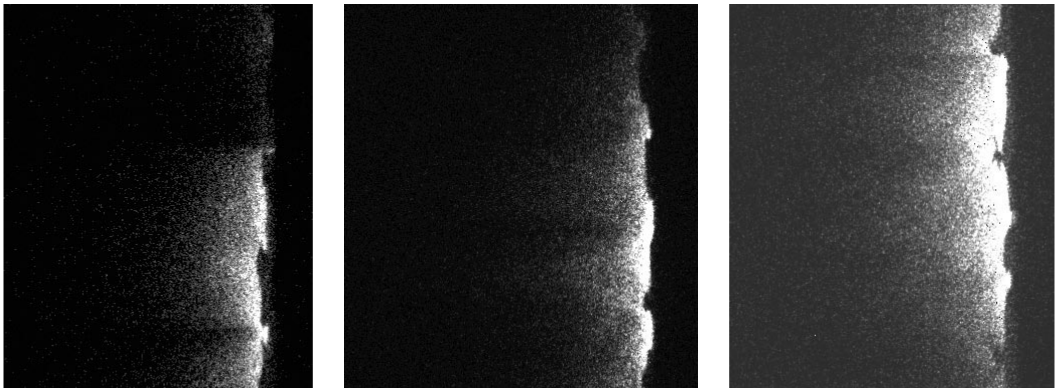

Shot 1411 Shot 1415 Shot 1416

Fig. 3 Images of OH fluorescence behind detonation fronts in stoichiometric hydrogen–oxygen mixture diluted with 80% argon, initial pressure 20 kPa.

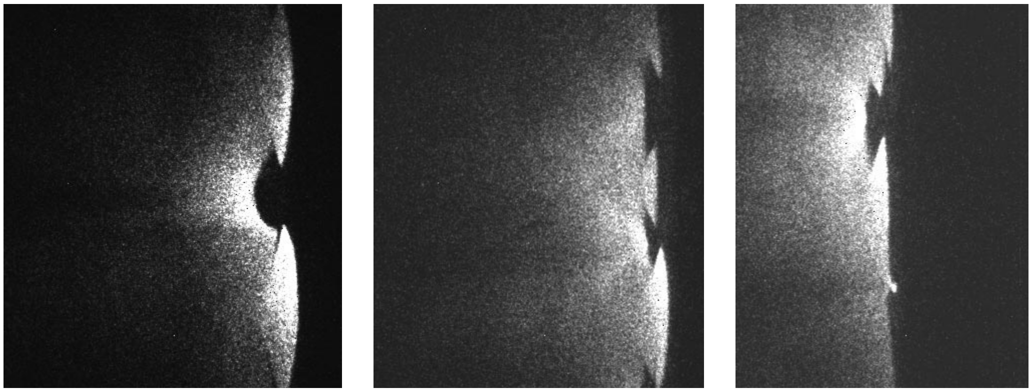

Shot 1419 Shot 1420 Shot 1417

Fig. 4 Images of OH fluorescence behind detonation fronts in stoichiometric hydrogen–oxygen mixture diluted with 85% argon, initial pressure 20 kPa.

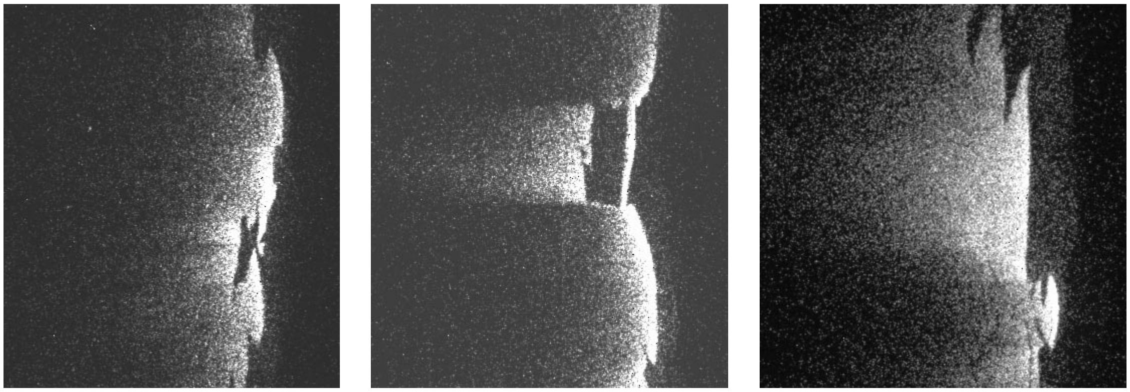

Shot 1426 Shot 1427 Shot 1428

Fig. 5 Images of OH fluorescence behind detonation fronts in stoichiometric hydrogen–oxygen mixture diluted with 60% nitrogen, initial pressure 20 kPa.

pronounced feature with a "keystone" shape is seen in shot 1419. Similar features appear in other images. An important point to note while examining these images is that the light sheet may not have intersected the cellular structure orthogonally, as can be seen from soot foils taken at the test section end-wall (Fig.2). That is, although the light sheet is aligned perpendicularly to the test section walls, the two planes of the detonation may not be orthogonal to these walls, potentially resulting in some three-dimensional effects in the images. In the facility used in these experiments, the detonation must transition from a tube with a round cross

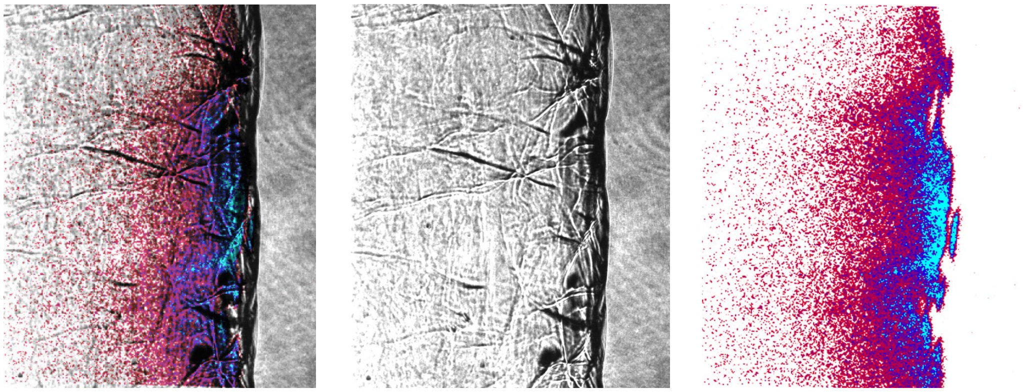

Shot 1432

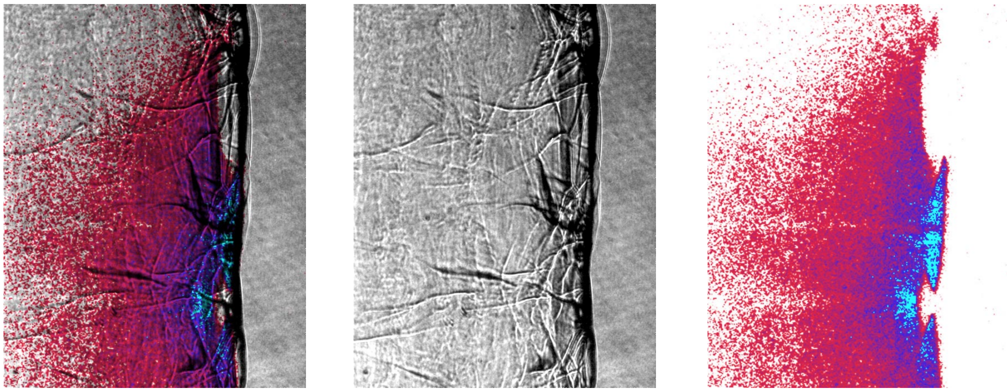

Shot 1433

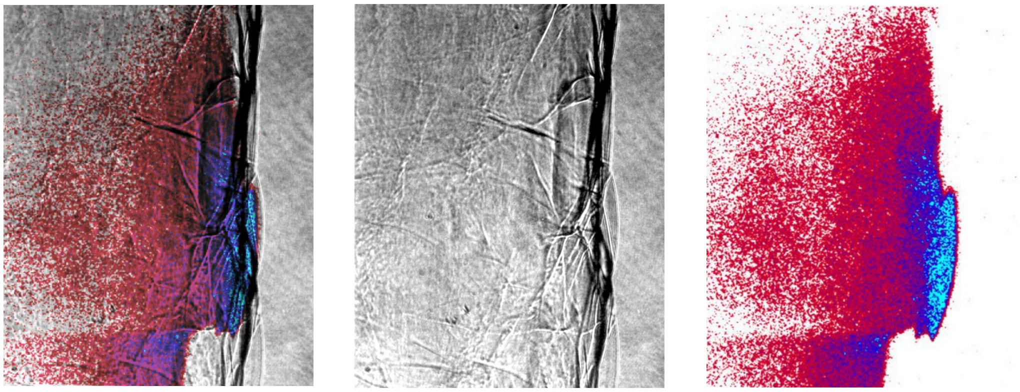

Shot 1434

(a) (b) (c)

Fig. 6 Simultaneous schlieren and OH fluorescence images behind detonation fronts in stoichiometric hydrogen–oxygen mixture diluted with 85% argon (shots 1432 and 1433) and 87% argon (shot 1434), initial pressure 20 kPa. (a) Overlay of PLIF and schlieren images (b) schlieren (c) PLIF.

section to a square test section via a cookie-cutter. This change in geometry may influence the orientation of the cell structure.

In Figs. 3–5, the shock location is not known but it can be inferred from the simulations and simultaneous schlieren and PLIF images to be just to the right of the OH emission front. We anticipate that the distance from the shock to the concentration front will be a strong function of shock strength and the clearly visible sudden changes or jumps in the location of the front must be associated with the instability of the detonation wave.

This is confirmed by the simultaneous schlieren and OH PLIF images shown in Fig. 6. Despite the masking effect of the three-dimensional nature of the transverse waves, it is clear that the changes in the OH concentration front location can be correlated directly with the density field changes visualized by the schlieren images. The variation in the OH concentration front location with shock velocity is confirmed by numerical simulations described subsequently.

The mixtures chosen in these experiments were in-

Table 1 Mixture parameters for the mixtures considered in these experiments, calculated with STANJAN.[13] The induction zone length, Δ_{ZND}, is defined by the location of maximum heat release; E_a/RT_{vN} is calculated as in Schultz and Shepherd.[14] Both these parameters are calculated using a detailed chemical mechanism.[15]

Composition	p_o (kPa)	U_{CJ} (m/s)	T_{vN} (K)	p_{vN} (MPa)	ρ_{vN} (kg/m^3)	Δ_{ZND} (mm)	E_a/RT_{vN}	λ (mm)
$2H_2$-O_2-7Ar	6.67	1618	1905	0.178	0.355	1.37	5.0	38±6
$2H_2$-O_2-12Ar	20	1518	1900	0.502	1.093	0.71	4.8	23±5
$2H_2$-O_2-17Ar	20	1415	1776	0.449	1.089	1.43	5.3	47±11
$2H_2$-O_2-20Ar	20	1357	1687	0.418	1.081	2.12	5.1	74±19
$2H_2$-O_2-4.5N_2	20	1875	1455	0.526	0.939	0.98	6.4	40±13

tended to investigate both regular (Ar diluted mixtures) and more irregular (N_2 diluted mixtures) cell structure to determine if there were corresponding differences in the chemical reaction zone structure and particularly, if differences could be seen in the mechanism by which combustion occurs. Previous work[16] has suggested that regular mixtures react by autoignition following shock compression, while the reaction zone of irregular mixtures is affected and possibly sustained by turbulence producing interactions, such as shock-shock or shock-shear layer interactions. We hope to be able to investigate these issues by directly visualizing the reaction zone structure of mixtures of varying cellular regularity. A list of mixture parameters is given in Table 1. Sooted foils from a 280 mm diameter detonation tube were used to measure the cell width in these mixtures and illustrate the differences in cellular regularity of the mixtures chosen (Fig. 7).

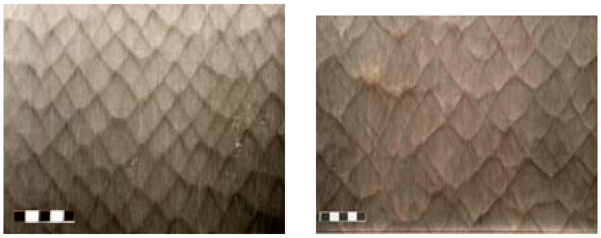

Fig. 7 Smoked foils obtained in a 280 mm diameter detonation tube for $2H_2$-O_2-12Ar (left) and $2H_2$-O_2-4.5N_2 (right), both at 20 kPa initial pressure. Flow is top to bottom. The scale shown corresponds to 50 mm. The Ar diluted mixture is an example of "excellent" regularity, while the N_2 diluted mixture has "poor" regularity of the cellular structure.

Numerical Simulation

Numerical simulations of two-dimensional detonations traveling at the Chapman-Jouguet velocity in $2H_2$-O_2-7Ar mixtures at an initial pressure of 6.7 kPa have been carried out by Eckett.[17] These simulations used a realistic reaction model and thermochemistry based on a detailed reaction mechanism. The chemical reactions were represented by an approximate four-dimensional manifold using the ILDM technique augmented with an induction time manifold for the initiation stage; details are provided in Eckett.[17] The numerical simulations used adaptive mesh refinement and an approximate Riemann solver (Roe-Glaister) to provide high resolution and accuracy. The ILDM manifold and the numerical solution technique were validated against several test cases and previously published results using the full detailed chemistry.

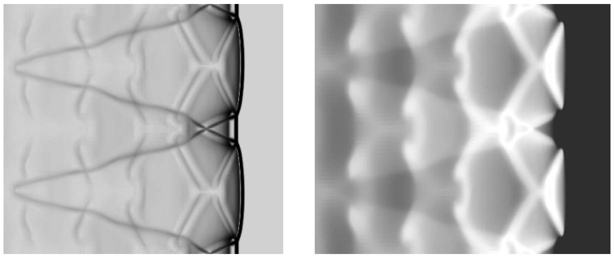

Density

OH mass fraction

Fig. 8 Results of numerical simulation of Chapman-Jouguet detonation in stoichiometric hydrogen–oxygen mixture diluted with 70% argon, initial pressure 6.7 kPa.

Simulated schlieren and OH mass fraction images are shown in Fig. 8. A close-up of the OH mass fraction and the key features of the detonation front are shown in Fig. 9. Several features can be observed in the close-up of the OH mass fraction. First, there are the obvious OH fronts closely following curved portions (Mach stems) of the leading shock wave. Second, on the centerline between the two Mach stems, there is a keystone-like feature which is bounded by the lead shock, the shear layer, and the OH front behind the incident wave (the geometrical configuration is discussed in more detail in the following section). Third, the decrease in mass fraction along the downstream edge of the slip lines can also be seen. There is a striking qualitative similarity between the overall appearance of the numerical simulation of OH mass fraction and the experimental images presented in Fig. 4. Keystone features are present in Fig. 3 but since the reaction zone is much shorter, they are not as distinct as in the 85% argon case. The features in Fig. 5 are much more irregular and pronounced than in the argon di-

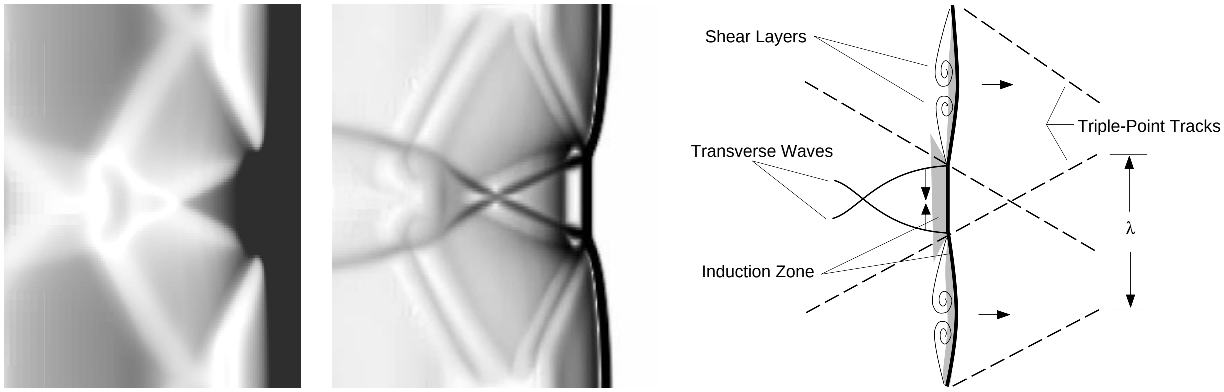

(a) (b) (c)

Fig. 9 (a) Close up of OH mass fraction contours shown in Fig. 8. (b) Close up of schlieren image of density field. (c) Schematic of detonation front features.

luted cases. This is consistent with the well-known observations of the irregularity of the cellular structure in nitrogen diluted cases as compared to the regular structure with large amounts of argon dilution.

It is important to note that the three-dimensional nature of the experimental studies, the nonuniformity of the light sheet, nonideal effects in the fluorescence process, and response of the camera will be important factors in determining the appearance of the OH front in the image. Given all of these issues, it is not surprising that the simulations do not exactly reproduce the observed shapes. Nevertheless, the results are startlingly similar and provide direct evidence of how the chemical reaction processes are affected by the detonation front instability.

Understanding the keystone regions requires investigating in detail the structure of the reaction zones behind the leading and transverse shock wave systems that make up the detonation front. Detailed analysis of the simulations can be used to obtain the variation of the leading shock front pressure and velocity through the cell; the results are shown in Fig. 10. The pressure and shock velocity variation indicates that the leading shock front velocity is a maximum value of about 1.3 U_{CJ} at the beginning of the cell ($x = x_o$), dropping sharply to about 0.93 U_{CJ} by the middle of the cell ($x - x_o = 0.5L$) and remaining nearly constant at this value until the collision of the transverse waves causes a rapid increase in the shock front velocity at the end of the cell (x-x_o = L). The observed range of leading shock velocities, $0.91 < U/U_{CJ} < 1.3$, is similar to that computed by Oran et al.[18] but smaller than has been experimentally observed by previous researchers[19–21] who studied marginal waves, for which the excursions in lead shock velocities are apparently much stronger. In addition, Gamezo et al.[22] calculate the amplitude of oscillation of lead shock velocity increases with increasing activation energy.

One key issue is the variation of the reaction rates behind the shock front. A common approach to this issue is to use a quasi-steady estimate of the reaction zone structure based on the instantaneous value of the leading shock velocity. Shown in Fig. 12 is an estimate of the thickness of the reaction zone length (based on the location of the maximum energy release rate) for the simulations shown in Fig. 8. The quasi-steady approach ignores the time-dependence or unsteadiness of the shock front and the possible effect on the reaction zone structure. The role of unsteadiness in detonation initiation has been considered by Eckett et al.[23] They show that the effect of a decaying wave is to increase the reaction zone thickness, and the amount of increase is a strong function of the rate of decay of the leading shock front. If the shock front decays faster than a critical value, then Eckett et al.[23] find that the unsteadiness can actually quench the reaction and cause the energy release to become completely decoupled from the shock front. Previous experimental and numerical studies on detonations have suggested that this occurs in some mixtures, resulting in unreacted "pockets" behind the detonation front.

Unreacted Gas Pockets

An unburned gas pocket is defined here as a region of unreacted gas that becomes detached from the main detonation front after the collision of two triple points. It should not be confused with the unreacted gas in the induction zone behind the incident wave which results in the keystone features observed in the PLIF images. unburned pockets are speculated to persist to a distance on the order of a cell dimension downstream of the main front and to be resolvable at the scale of the cell width.

"Islands" of unreacted gas that become isolated downstream of the main detonation front were first discussed by Subbotin[24] in his schlieren study of the detonation structure of regular and irregular mixtures. In an irregular mixture, CH_4-$2O_2$-0.2Air [*], he concluded from polar calculations based on the observed

---

[*] stoichiometric CH_4-O_2 diluted with 6% air

wave angles that the transverse wave configurations were usually unreactive and reported that unburned islands of gas were formed. In these irregular methane mixtures, the unburned islands were fragmented by the fine scale cellular structure. These detonations were reported to be self-sustaining. In a regular mixture, $2H_2$-O_2-3Ar, he reported reactive transverse waves and no pocket formation except when the initial pressure was lowered sufficiently for the detonation to become marginal. In these marginal cases, he concluded both reactive and unreactive transverse wave configurations were observed. He showed schematically how regular, triangular-shaped, unburned gas islands could be formed by the collision of unreactive transverse waves. He noted that in these mixtures, the detonation was unstable and failing. Subbotin's conclusions about the reaction zone structure, while very interesting, are based on (often unpublished) schlieren images, and furthermore, result from experiments conducted in a very narrow (4.7 mm) channel which was also rather short (1.4 m long), making it difficult to determine the stability of the detonation.

In 1982, Edwards[25] took schlieren images in a $2H_2$-O_2-4.5%Ar mixture, in a narrow (6.3 mm) channel, and observed density gradients of irregular regions of gas on the order of one cell width downstream of the front. An accompanying numerical simulation of a detonation near its initiation limit in this mixture shows a region of increased induction time left isolated after the collision of an unreactive triple point with an axis of symmetry. In more recent numerical simulations, Gamezo et al.[26] report that unburned pockets are commonly observed and conclude mixtures with low activation energies (E_a/RT_{ZND}=2.1) show unburned pockets that are triangular in shape with indistinct boundaries while higher activation energy (E_a/RT_{ZND}=7.4) mixtures have distinct, irregular pockets which survive further downstream. Gamezo et al.[22] believe the mechanism by which the pockets are consumed also varies with the activation energy of the mixture. Pockets in low activation energy mixtures react by auto-ignition after shock compression, while pockets in irregular mixtures are consumed by heat and mass exchange with neighbouring hot gases through diffusion and turbulence (although diffusion is numerical and turbulence is not resolved!).

Sharpe[28] observes the collision of two transverse wave configurations in which the secondary triple point becomes detached from the front before collision. The triple point configuration that remains attached to the front is not strong enough to consume the unreacted gas upon collision, resulting in an unburned pocket. Sharpe also shows that numerical resolution can play an important role in determining the structure of the triple point and the presence of unburned regions with insufficient resolution resulting in an artificially accelerated reaction rate.

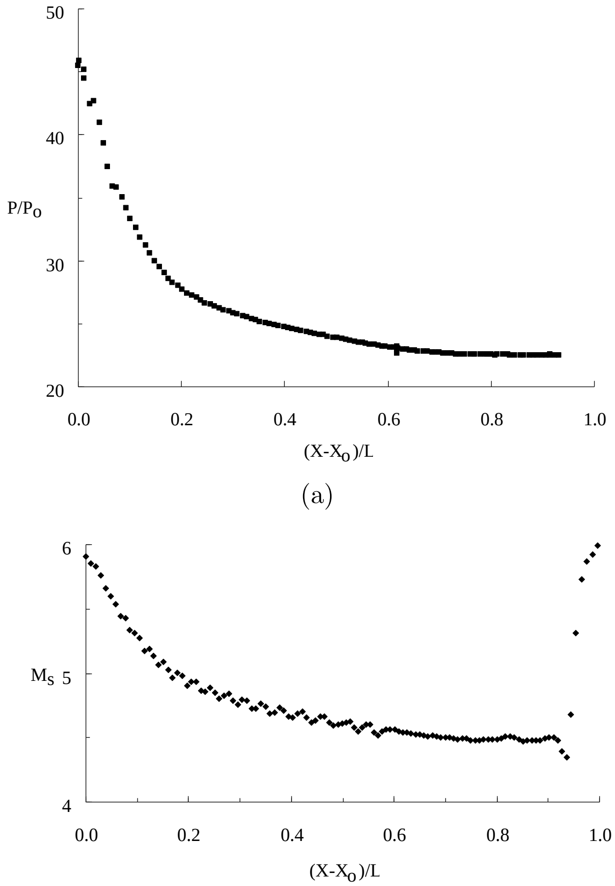

(a)

(b)

Fig. 10 (a) Pressure behind leading shock wave along centerline of detonation cells for the simulations of Fig. 8. These results were obtained by interrogation of the pressure field in the fully-developed regime, see Fig 3.39 in Eckett.[17] (b) Mach number of leading shock front along the centerline of the detonation cells for the simulations of Fig. 8. Shock velocities were obtained by differentiation of the smoothed wave trajectories obtained by interrogating the solution field in the fully-developed regime, see Fig. 3.39 in Eckett.[17]

All previous investigations of unreacted pockets, both experimental and numerical, have been carried out in the special case of essentially two-dimensional flows, commonly on marginal detonations. unburned pockets have been postulated to appear in cases where the transverse waves are weak and do not consume the reactants behind the incident wave during the triple point collision. Although from shock-polar analysis as well as from the shape of the keystone region (see section below), we conclude that in the case of the $2H_2$-O_2-Ar mixtures we studied, the transverse waves are weak (M_T ≈1.2) and unreactive, no such pockets were observed in the present experiments. The PLIF signal intensity decays with distance from the front, so

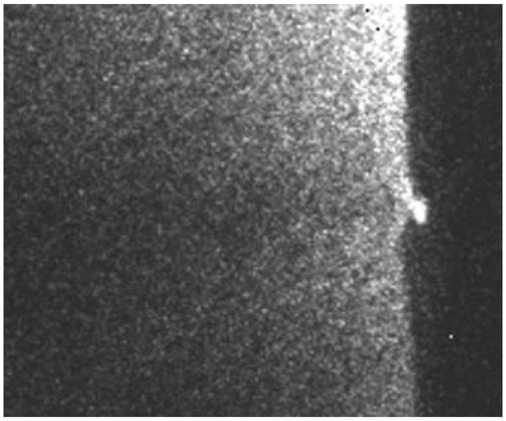

Fig. 11 Detail from shot 1417, $2H_2$-O_2-17Ar at 20 kPa, showing a new Mach stem formed after a triple point collision. No unreacted pockets are evident.

that small differences in reactivity may be difficult to image more than 2-3 cm downstream of the reaction zone. However, if unreacted pockets exist, we would expect to see evidence of their formation close to the front. The PLIF image from shot 1417, shown in detail in Fig. 11, shows what appears to be a new Mach stem forming just after a triple point collision, and no unreacted region is visible.

In the N_2 diluted mixtures studied, some unusual features are observed (see, for example, Shot 1427); however these do not have the structure previously associated with unburned pockets. We attribute these features to the relative orientation of the light sheet to the planes of the detonation cells. The transition the detonation must make from a round tube to the square test section may create this three-dimensional effect. A study with sooted foils located along the length of the test section recorded the transition in cellular structure from spinning to orthogonal, and found N_2 diluted mixtures require a greater distance for the cellular structure to become orthogonal, resulting in more pronounced three-dimensional effects in these mixtures.

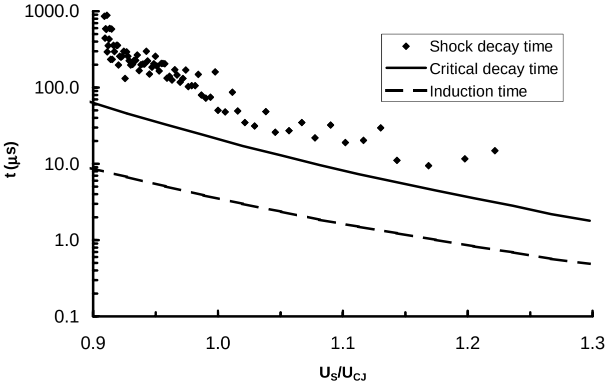

Fig. 12 Time scales in detonation cell for simulations of Fig. 8. The shock decay times were obtained by numerical differentiation of smooth data shown in Fig. 10b. The induction times are based on ZND simulations based on the instantaneous values of the leading shock velocity. The critical decay time concept is discussed in Eckett et al.[27]

Sharpe's observations about numerical resolution[28] may explain the absence of pockets in our numerical simulations. However, we can examine the potential for pocket formation in the simulations of Eckett[17] by computing the shock decay time through numerical differentiation of the data in Fig. 10b. This is compared to the computed critical decay rates, as defined by Eckett,[23] in Fig. 12. We would not expect any decoupling or pocket formation since the shock decay time is less than the critical shock decay time throughout the entire cell. Also, on this basis, subsequent computations of the reaction zone structure will use the quasi-steady approximation for simplicity.

Triple Point Analysis

Triple point configurations through a detonation cell have been investigated experimentallly, theoretically, and numerically by various researchers. Progress has been made towards determining the triple point structure at different locations through the cell for varying mixtures in varying geometries, resulting in a wide spectrum of results.

The strength and reactivity of transverse waves, at least in the vicinity of the triple point, may be calculated by polar analysis and zero-dimensional reaction zone models. From this type of analysis, we can order some sample mixtures in terms of their expected transverse wave strengths in order to have a loose classification of the mixtures studied in the present experiments. Shock polars are calculated using the oblique shock jump relations. Details of this type of calculation may be found in several previous works.[24,30–32] Two parameters are required: the incoming flow angle which is obtained from the soot foil track angle, and the incoming flow velocity which is calculated along the cell centerline in the numerical simulation. A sample calculation, together with a comparison with a corresponding numerical schlieren image, is shown in Fig. 13. These calculations have several simplifications. The flow is assumed to be a perfect gas and to be steady in the frame of the triple point. The waves are assumed to be straight, an assumption that is more valid for nonreactive than reactive flow, and a probable effect of the chemistry will be to produce some wave curvature. The oscillation in centerline velocity is assumed to be the same for all mixtures although it should be noted that Gamezo et al.[22] calculate larger oscillations in the case of mixtures with higher activation energies.

In general, we calculate that Ar diluted mixtures

Mixture	$C_{p_{vN}}$ kJ/kg-K	c_1 m/s	M_T	$(p_3 - p_2)/p_2$	E_a/RT_{vN}	τ_T μs	τ_T/τ_I
$2H_2$-O_2	2.87	573	1.40	0.376	5.5	0.245	0.540
$2H_2$-O_2-3Ar	1.08	379	1.30	0.357	5.4	0.293	0.548
$2H_2$-O_2-12Ar	0.69	339	1.24	0.341	5.2	0.927	0.514
$2H_2$-O_2-$3N_2$	1.72	416	1.40	0.376	6.1	0.873	0.536
$2H_2$-O_2-CO_2	1.96	411	1.37	0.379	10.2	1.314	0.479
CH_4-$2O_2$	2.09	355	1.51	0.385	11.7	1.435	0.422
C_2H_4-$3O_2$	1.86	326	1.55	0.388	6.8	0.367	0.527
C_3H_8-$5O_2$	2.01	306	1.65	0.395	10.6	0.274	0.436

Table 2 Mixture parameters and transverse wave strengths for some sample mixtures, calculated in the vicinity of a primary triple point. All calculations are for mixtures at 20kPa as transverse wave strength is not a strong function of initial presssure until the detonation becomes marginal. Activation energy and induction time calculations use the detailed chemical mechansim of Konnov,[29] previously validated against shock tube ignition delay data.[14]

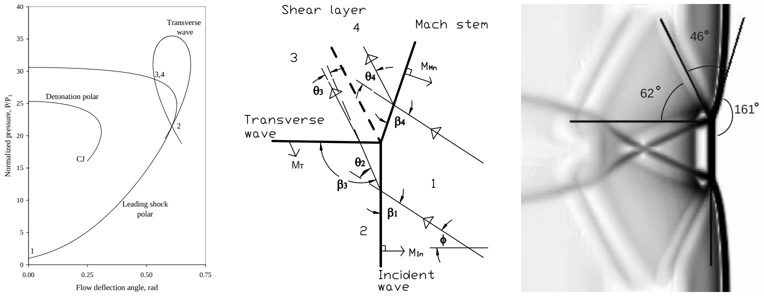

Fig. 13 Shock and detonation polar calculations for stoichiometric hydrogen–oxygen mixture diluted with 70% argon, initial pressure 6.67 kPa, $x - x_o$= 0.91L, ϕ=33°. A comparison with the a numerical schlieren image at the same location in the cell is also shown.

have weaker transverse waves than N_2 diluted mixtures which are weaker in turn than mixtures with CO_2 dilution for the same percent diluent. Hydrocarbons have stronger transverse waves than H_2, with transverse wave strength increasing with carbon content for methane, ethylene and propane. The reactivity of the transverse waves is ordered by τ_T/τ_I, the ratio of the constant volume induction time, τ_T, for a particle passing through the incident and then immediately through the transverse wave (particle 2 in Fig. 14), normalized by the induction time behind the incident wave, τ_I. This parameter has a range $0 \leq \tau_T/\tau_I \leq 1$, with values close to zero corresponding to a very short induction time behind the transverse wave, so that the transverse wave may be called reactive, and one corresponding to a relatively long induction time, meaning the transverse wave has a negligible effect on the reaction. For all the mixtures shown here, τ_T/τ_I is about 0.5. Our calculations of the induction time behind the transverse wave, τ_T, show the shortest time in the case of $2H_2$-O_2 and the longest in CH_4-$2O_2$. This trend agrees with the observations of Subbotin,[24] who studied self-sustaining waves in a narrow channel and classified transverse waves in $2H_2$-O_2-3Ar as reactive while transverse waves in CH_4-$2O_2$-0.2Air were unreactive. As can be seen from the table, the mixtures considered in these experiments have transverse waves with Mach number around 1.2 and strength, defined as the normalized pressure jump across the wave, $(p_3 - p_2)/p_2$, of about 0.3. Strehlow and Biller[33] found wave strengths ranging from 0.22 to 1.2 in a study with various mixtures, so the transverse waves in the present experiments are at the lower end of this range.

ZND and constant volume explosion calculations (see Shepherd[34]) are used to estimate the OH mole fraction contours in the region of the triple point. A detailed chemical mechanism,[15] previously validated against shock tube ignition delay data,[14] was used. The orthogonal component of the flow across the incident wave was used in a ZND calculation to obtain the induction distance, defined as the location of the rise in OH mole fraction. A similar calculation was made across the Mach stem. The dependance of the location of the rise in OH mole fraction, and therefore, of the induction distance, on the varying shock strength in different parts of the front, results in the discontinous keystone structure we see in the PLIF images.

The induction time behind the transverse wave was calculated with a constant volume explosion assumption. The induction distance was then found from the post-shock flow velocity projected at the calculated flow angle behind the transverse wave. This was done for several particle paths with initial flow conditions obtained from the ZND calculations behind the incident wave to simulate the partially reacted flow. A sample calculation is shown in Fig. 14. For this simple analysis, the transverse wave is assumed to be unaffected by the reaction zones behind it and behind the incident wave; the transverse wave Mach number is kept constant at the value calculated at the triple point. These calculations show quantitative agreement with the PLIF images, although the location of the shock structure must be estimated, and with numerical simulations.

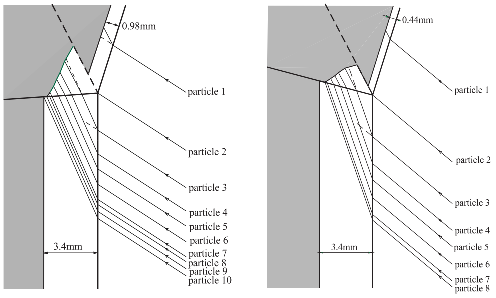

Fig. 14 Prediction of the keystone region shape for stoichiometric hydrogen–oxygen with 85% argon dilution for $\phi = 33^\circ$ (left) and $\phi = 40^\circ$ (right). These predictions are based on the idealized model of the triple point configuration discussed in the text and estimates of the OH mole fraction using simple zero and one-dimensional reaction zone models. The transverse wave was assumed to remain straight with constant Mach number. The edge of the reaction zone is defined as the location of the contour χ_{OH}=0.005. The choice of OH contour χ_{OH}=0.005 is arbitrary, but as the OH rise is exponential, the features remain qualitatively the same irrespective of which value is chosen.

Fig. 14 makes clear the role the transverse wave plays in the structure of the reaction zone. In the absence of a transverse wave, the keystone shape would have a straight contour with no discontinuity other than that across the shear layer. Such shapes can be seen in the PLIF images, for example in Fig. 4, shot 1420, from which we can conclude the transverse waves have a modest effect on the flow and do not appear to play an essential role in accelerating the reaction rate.

The role of transverse waves

A key scientific question is: What is the role of the transverse waves in detonation propagation? Two extreme points of view are:

1. The transverse waves are simply manifestations of instability and do not play an essential role in the propagation mechanism. The main portion of the reaction is due to the leading shock waves and only a small fraction of the reactants pass through the transverse wave.
2. Transverse waves are essential to detonation propagation. The transverse waves and interactions of transverse waves provide high-temperature regions ("hot spots") that serve as reaction centers. The majority of the chemical reaction takes place behind the transverse waves or is associated with reaction centers.

We have examined only one fuel-oxidizer combination and two diluents in the present study. For those mixtures, we observe behavior that is closer to the first point of view: the transverse waves play a nonessential role in detonation propagation. Mixtures with very different thermodynamic and kinetic parameters need to be examined to determine if the second type of behavior is possible. It has been suggested that high activation energies and certain hydrocarbon fuels without inert gas dilution are more representative of the second class of mixtures. Further studies are in progress in our laboratory to examine a wider range of mixtures and determine the chemical structure of the detonation front for those cases.

The present study was restricted to mixtures with modest activation energy (see Table 1) but included mixtures with a wide range of cellular regularity. The highly argon diluted mixtures are well known to have "excellent regularity" while the nitrogen diluted mixtures are classified[35] as having "fair" regularity (see Fig. 7). It is important to note that our OH PLIF visualizations of these two mixtures do not show a dramatic difference in the structure of the front that would indicate a qualitative difference in the role of the transverse waves. We do see a more irregular structure of the OH front in the nitrogen diluted cases than in the argon diluted cases, but we do not see any indication of pockets or inclusions of unburned material behind the leading shock front. We conclude that the irregularity is simply due to the spontaneous generation and decay of triple points along the front, and the transverse waves play a similar role for both diluents.

From our simple considerations about triple point structure, we find a modest decrease in the reaction time behind the transverse wave structures that are consistent with our present observations. The reaction time for the fluid elements closest to the triple point will decrease about a factor of two due to the increase in temperature across the transverse wave. While this affects the details of the keystone shape, it does not seem appropriate to refer to the transverse waves as "reactive" in this case. However, it is clear that the possibility of reactive transverse waves has been demonstrated by computations and experiments in marginal propagation situations. Further studies are needed with other mixtures to determine if reactive transverse waves have a role in "ordinary" (near CJ) detonations.

Conclusions

Experimental observations have been made of the reaction zone structure in propagating detonations. H_2-O_2-diluent mixtures representative of regular and irregular cell structures were studied. PLIF images reveal distinctive keystone features associated with the triple points. Differences in cellular structure regularity are seen in the different mixtures, with N_2 diluted mixtures sometimes exhibiting unexpected features that may be attributed to three-dimensional effects.

The local structure of the triple point is analysed by an unreactive shock polar calculation, revealing the keystone features are due to a discontinuity in reactivity across the shear layer. Also from this analysis and from the images themselves, we conclude the transverse waves have little influence on the reaction, particularly in the case of the Ar diluted mixtures.

Previous numerical work has suggested that in the case of mixtures with low-amplitude transverse waves, pockets of unreacted gas may be formed if the transverse waves do not consume the unreacted gas behind the incident wave during triple point collision. A region of unreacted gas becomes isolated from the front and may persist a cell length downstream. In all images obtained in the present study, no detached pockets of gas are seen within the field of view of the measurement.

Our study has examined a limited range of mixtures and initial conditions. Other triple point configurations, reactive transverse waves, and pockets may be possible for different mixtures with a wider range of chemical and thermodynamic properties. Experiments are in progress to examine these situations.

Acknowledgements

This work was partially supported by the Office of Naval Research Multidisciplinary University Research Initiative *Multidisciplinary Study of Pulse Detonation Engine* (grant 00014-99-1-0744, sub-contract 1686-ONR-0744).

References

[1] Andresen, P., Reckers, W., Wagner, H., Dabora, E., and Voges, H., "The Structure of Gaseous Detonations as Revealed by Laser-Induced Fluourescence of the OH-Radical," *Zeitschrift fur Physicalische Chemie Neue Folge*, Vol. 175, 1992, pp. 129–143.

[2] Anderson, T. and Dabora, E., "Measurements of Normal Detonation Wave Structure using Rayleigh Scattering," *24th Symposium (International) on Combustion*, The Combustion Institute, Pittsburgh, PA, 1992, pp. 1853–1860.

[3] Eder, A., *Brennerverhalten schnallnaher und überschallschneller Wasserstoff-Luft Flammen*, Ph.D. thesis, Technische Universität München, Munich, Germany, January 2001.

[4] Eckbreth, A. C., *Laser Diagnostics for Combustion Temperature and Species*, Abacus Press, Cambridge, MA, 1988.

[5] Toshimitsu, K., Matsuo, A., Kamel, M., Morris, C., and Hanson, R., "Numerical simulations and planar laser-induced fluorescence imaging results of hypersonic reactive flows," *Journal of Propulsion and Power*, Vol. 16, No. 1, 2000, pp. 16–21.

[6] Morris, C., Kamel, M., and Hanson, R., "Shock-Induced Combustion in High-Speed Wedge Flows," *27th Symposium (International) on Combustion*, The Combustion Institute, Pittsburgh, PA, 1998, pp. 2157–2164.

[7] McMillan, B., Lee, M., Paul, P., and Hanson, R., "Planar Laser-Induced Fluorescence of Shock-Induced Ignition," *23th Symposium (International) on Combustion*, The Combustion Institute, Pittsburgh, PA, 1990, pp. 1909–1919.

[8] Akbar, R., *Mach Reflection of Gaseous Detonations*, Ph.D. thesis, Rensselaer Polytechnic Institute, Troy, New York, August 1997.

[9] Kaneshige, M. J., *Gaseous Detonation Initiation and Stabilization by Hypervelocity Projectiles*, Ph.D. thesis, California Institute of Technology, Pasadena, California, January 1999.

[10] Luque, J. and Crosley, D. R., "LIFBASE Database and Spectral Simulation Program (Version 1.5)," Tech. Rep. MP 99-009, SRI International, 1999, http://www.sri.com/cem/lifbase.

[11] Dyer, M. and Crosley, D., "Two-dimensional imaging of OH laser-induced fluorescence in a flame," *Optics Letters*, Vol. 7, No. 8, 1982, pp. 382–384.

[12] Seitzman, J. and Hanson, R., "Comparison of excitation techniques for quantitative fluorescence imaging of reacting flows," *AIAA Journal*, Vol. 31, No. 3, 1993, pp. 513–519.

[13] Reynolds, W., "The element potential for chemical equilibrium analysis: implementation in the interactive program STANJAN," Tech. Rep. A-3991, Dept. of Mechanical Engineering, Stanford University, Stanford, CA, January 1986.

[14] Schultz, E. and Shepherd, J., "Validation of detailed reaction mechanisms for detonation simulation," Tech. Rep. FM99-5, Graduate Aeronautical Laboratories: California Institute of Technology, 2000.

[15] Warnatz, J. and Karbach, V., "C2 mechanism for methane-air combustion," *http://www.ca.sandia.gov/tdf/3rdWorkshop/ch4mech.html*, 1997.

[16] Lee, J., "Dynamic Structure of Gaseous Detonation," *Fluid Mechanics and its Applications v.5 Dynamic structure of detonation in gaseous and dispersed media*, Kluwer Academic Publishers, Netherlands, 1991, p. 1.

[17] Eckett, C. A., *Numerical and Analytical Studies of the Dynamics of Gaseous Detonations*, Ph.D. thesis, California Institute of Technology, Pasadena, California, September 2000.

[18] Oran, E. S., Weber, Jr., J. W., Stefaniw, E. I., Lefebvre, M. H., and Anderson, Jr., J. D., "A Numerical Study of a Two-Dimensional H_2–O_2–Ar Detonation Using a Detailed Chemical Reaction Model," *Combust. Flame*, Vol. 113, 1998, pp. 147–163.

[19] Voitsekhovskii, B., Mitrofanov, V., and Topchian, M., "Struktura fronta detonastii i gaza," *Akad. Nauk., SSSR, Novosibirsk*, 1963, Translation: The structure of a detonation front in gases Rep. FTD-MT-64-527, Foreign Technology Division, Wright-Patterson A.F.B., Ohio,(1966).

[20] Lundstrom, E. and Oppenheim, A., "On the influence of non-steadiness on the thickness of the detonation wave," *Proc. Roy. Soc. A*, Vol. 310, 1969, pp. 463–478.

[21] Strehlow, R. and Crooker, A., "The structure of marginal detonation waves," *Acta Astronautica*, Vol. 1, 1974, pp. 303–315.

[22] Gamezo, V., Desbordes, D., and Oran, E., "Formation and evolution of two-dimensional cellular detonations," *Combust. Flame*, Vol. 116, 1999, pp. 154–165.

[23] Eckett, C., Quirk, J., and Shepherd, J., "An Analytical model for direct initiation of gaseous detonations," *Proceedings of the 21st International Symposium on Shock Waves*, edited by A. Houwing, R. Boyce, P. Danehy, M. Hannemann, J. Kurtz, T. McIntyre, S. McMahon, D. Mee, A. Paull, R. Sandeman, and H. Tanno, Vol. 1, 1998, pp. 383–388.

[24] Subbotin, V., “Two kinds of transverse wave structures in multi-front detonation,” *Fizika Goreniya i Vzryva*, Vol. 11, No. 1, 1975, pp. 96–102.

[25] Oran, E., Young, T., Boris, J., Picone, J., and Edwards, D., “A Study of Detonation Structure: The Formation of Unreacted Gas Pockets,” *19th Symposium (International) on Combustion*, The Combustion Institute, Pittsburgh, PA, 1982, pp. 573–582.

[26] Gamezo, V., Desbordes, D., and Oran, E., “Two-dimensional reactive flow dynamics in cellular detonation waves,” *Shock Waves*, Vol. 9, 1999, pp. 11–17.

[27] Eckett, C., Quirk, J., and Shepherd, J., “The role of unsteadiness in direct initiation of gaseous detonation,” *Journal of Fluid Mechanics*, Vol. 421, 2000, pp. 147–183.

[28] Sharpe, G., “Transverse waves in numerical simulations of cellular detonations,” *submitted to J. Fluid Mech.*, 2001.

[29] Konnov, A., “Detailed reaction mechanism for small hydrocarbon combustion. Release 4.0,” *http://homepages.vub.ac.be/ akonnov*, 1998.

[30] Oppenheim, A., Smolen, J., and Zajac, L., “Vector polar method for the analysis of wave intersections,” *Combust. Flame*, Vol. 12, 1968, pp. 63–76.

[31] Urtiew, P., “Reflections of wave intersections in marginal detonations.” *Astronautica Acta*, Vol. 15, 1970, pp. 335–343.

[32] Barthel, H., “Reaction zone-shock front coupling in detonations,” *Phys. Fluids*, Vol. 15, No. 1, 1972, pp. 43–50.

[33] Strehlow, R. and Biller, J., “On the strength of transverse waves in gaseous detonations,” *Combust. Flame*, Vol. 13, 1969, pp. 577–582.

[34] Shepherd, J., “The chemical kinetics of hydrogen-air-diluent detonations,” *Prog. Astronaut. Aeronaut.*, Vol. 106, 1986, pp. 263–293.

[35] Libouton, J., Jacques, A., and Van Tiggelen, P., “Cinétique, structure et entretien des ondes de détonation,” *Actes du Colloque International Berthelot-Vieille-Mallard-Le Chatelier*, Vol. 2, 1981, pp. 437–442, Bordeaux.